Supporting Information

Colavin et al. 10.1073/pnas.1317061111

SI Text

Calculation of Filament Bending Rigidity. We describe the bending of actin homolog MreB filaments using three Euler angles, as shown in Fig. 4*A* of the main text. The angles are defined as follows. The first angle (θ_1) corresponds to relative bending around the largest principal axis of inertia of each monomer. The third angle (θ_3) corresponds to filament twisting around the axis from the (−) subunit center-of-mass to the (+) subunit center-of-mass in the straight protofilament crystal structure (1). The second Euler angle (θ_2) corresponds to bending around the axis defined by the vector in the direction of the cross-product of the vectors defining θ_1 and θ_3.

To determine the bending rigidity of an MreB protofilament from dimer simulations (referred to as F-MreB by analogy with actin), we fit the distribution of the equilibrated final 30 ns of F-MreB Mg^{2+} simulations (6 and 7 in Table S1) to a Gaussian. A good fit indicates a harmonic energy of the form

$$U(\theta_i) = \frac{k_B T}{2\sigma_i^2}(\theta_i - \theta_i)^2 = \frac{E_i I l}{2}(\kappa_i - \kappa_i)^2,$$

where σ_i and θ_i are the SD and mean of the Gaussian fit, E_i is the elastic Young's modulus, I is the second moment of area (estimated as $\pi r^4/4$, where $r \approx 1.75$ nm), l is the subunit length (≈ 5.1 nm), and $\kappa_i = \theta_i / l$ is the curvature. Values for the bending orientations and stiffnesses ($k_i = k_B T/\sigma_i^2$) for ADP- and ATP-bound F-MreB simulations are given in Table S3.

Buried Solvent-Accessible Surface Area As a Measure of Subunit–Subunit Contact Stability. To measure the stability of the contact between subunits in our dimer simulations, we measured the buried solvent-accessible surface area (SASA), which is the area on the surface of two subunits of a dimer that water cannot access. The buried SASA is defined as the addition of the full SASA for the (+) and (−) subunits minus the SASA for both subunits (2). This measure has similar distributions and means for ATP- and ADP-bound simulations (Fig. S4), despite the difference in relative bending between monomers, indicating that contact between MreB subunits is stable.

Young's Modulus of the MreB Filament. We measured the distance between the subunit centers-of-mass as a function of time in our dimer simulations (Fig. S3). The distribution was Gaussian, and hence the stretching stiffness can be extracted (2) from the harmonic energy

$$U(l) = \frac{k_B T}{2\sigma^2}(l - l)^2 = \frac{k_s}{2}(l - l)^2,$$

where $k_s = k_B T/\sigma^2$ is the effective spring constant of the system along the filament length. Hooke's law for a linear spring is related to the Young's modulus of a rod-like filament by

$$E = \frac{\text{stress}}{\text{strain}} = \frac{F/A_0}{\Delta L/L_0} = \frac{FL_0}{A_0 L}$$

$$\Rightarrow F = -\left(\frac{EA_0}{L_0}\right)\Delta L = -k_s x$$

$$\Rightarrow E = k_s\left(\frac{L_0}{A_0}\right),$$

where L_0 and A_0 are the initial length and cross-sectional area of the spring system, which we measured for MreB to be ∼51.1 Å and 803 $Å^2$, respectively. For both ATP- and ADP-bound simulations, $\sigma = 0.4$ Å, corresponding to a stiffness of $k_s = 2{,}700$ N/m = 6.5 $k_B T/Å^2$ and a Young's modulus of 1.7 GPa.

Interfacial and Nucleotide-Proximal Residues of MreB Are Highly Conserved in MreB from Other Gram-Negative Model Organisms. Because the only published crystal structure of MreB is from *Thermotoga maritima*, we compared its sequence with MreB from other Gram-negative model bacteria *Escherichia coli* and *Caulobacter crescentus.* From the aligned sequences, we identified 30 residues that are conserved in *C. crescentus* and *E. coli* but not in *T. maritima*. None of these residues is located in the nucleotide-binding pocket, and only two are located within 5 Å of the crystal polymerization interface. The strong similarity of residues in these regions suggests that MreB from other Gram-negative species will exhibit similar conformational dynamics as reported here for *T. maritima* MreB.

1. van den Ent F, Amos LA, Löwe J (2001) Prokaryotic origin of the actin cytoskeleton. *Nature* 413(6851):39–44.

2. Hsin J, Gopinathan A, Huang KC (2012) Nucleotide-dependent conformations of FtsZ dimers and force generation observed through molecular dynamics simulations. *Proc Natl Acad Sci USA* 109(24):9432–9437.

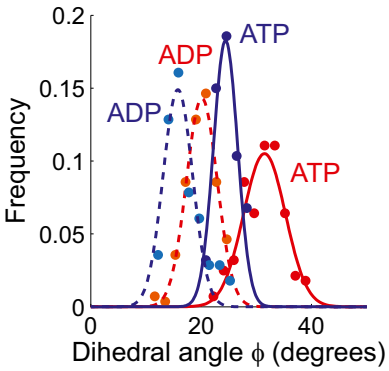

Fig. S1. Polymerization and nucleotide-dependent flattening of MreB. The flattening of monomers (referred to as G-MreB by analogy with actin), as measured by the dihedral angle, depends both on nucleotide identity and on polymerization state. Polymerization flattens the monomer, as does replacement of ATP with ADP. The effects are additive, as shown by the equilibrium distributions of dihedral angles in each condition. F-MreB and G-MreB simulation distributions are shown as dashed and solid lines, respectively.

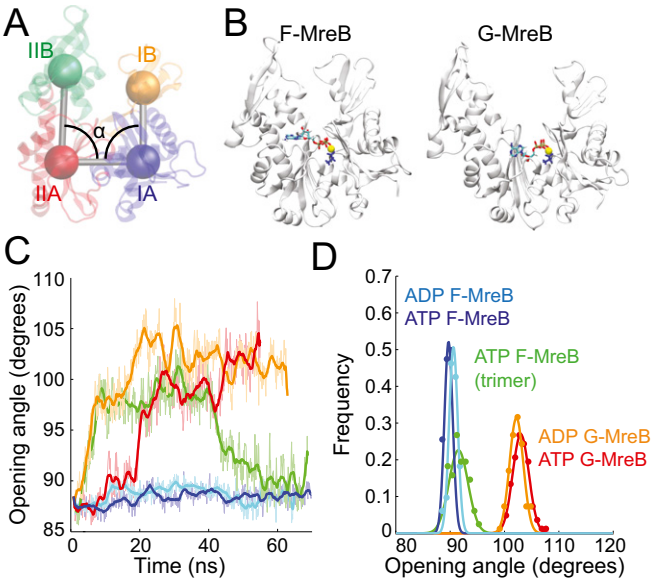

Fig. S2. Opening of monomer in G-MreB simulations. (*A* and *B*) Simulations of G-MreB immediately exhibited large-scale monomer opening, as captured by α, the average of the two inner angles of the coarse-grained description of MreB. In contrast, both subunits in F-MreB dimer simulations remained closed in the vast majority of simulations. (*C* and *D*) In a trimer simulation of F-MreB bound to ATP (green), the (+) subunit initially opens and then later stabilizes in a closed state. No (–) subunits in our dimer simulations ever opened, suggesting that subsequent polymerization stabilizes the closed state.

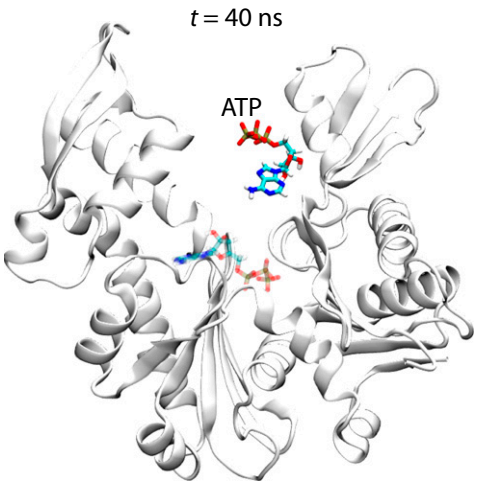

Fig. S3. ATP requires chelation for γ-phosphate stability. In the absence of chelating Mg^{2+}, the γ-phosphate flips out of the structure. In some repeat simulations, this change led to full dissociation of ATP from the binding pocket of MreB. A snapshot of this type of simulation is shown with transparent ATP in its initial configuration, and its subsequent position 40 ns into the simulation.

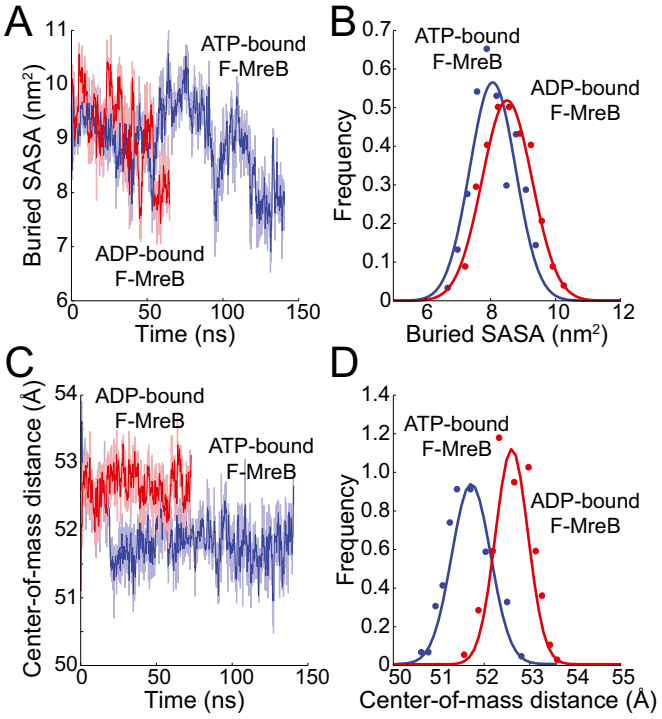

Fig. S4. Stability of subunit contact. (*A*) Simulations with different bound nucleotides exhibited similar buried solvent-accessible surface areas (buried SASA). Higher values of buried SASA indicate more contact between subunits. (*C*) Stability and elastic stiffness of the distance between dimer subunit center-of-masses. (*B* and *D*) Distributions and Gaussian fits of the last 30 ns of each simulation in *A* and *C*, respectively.

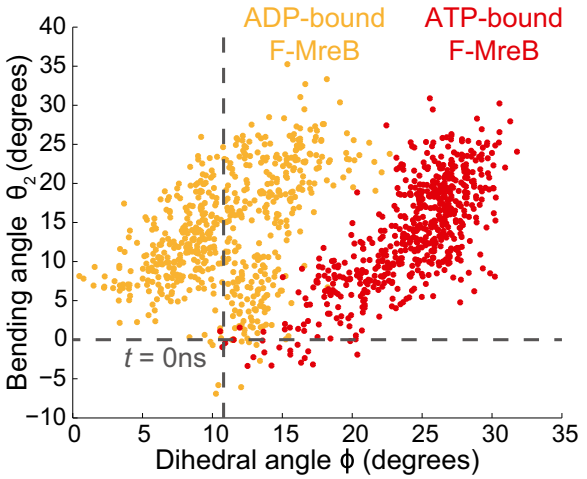

Fig. S5. Coupling of intramolecular flattening with intermolecular bending is nucleotide-dependent. Simulations of F-MreB bound to either ATP or ADP exhibited strong coupling between the intramolecular flattening of the (–) monomer and the bending of the dimer. The nucleotide identity shifted the relative coupling of these two order parameters. A scatter plot of the values measured every 0.1 ns in 60-ns F-MreB simulations bound to either ATP or ADP (red and orange, respectively) reveals that ATP- and ADP-bound MreB dimers both exhibit this coupling but occupy different domains. Dashed lines represent values of the MreB crystal structure.

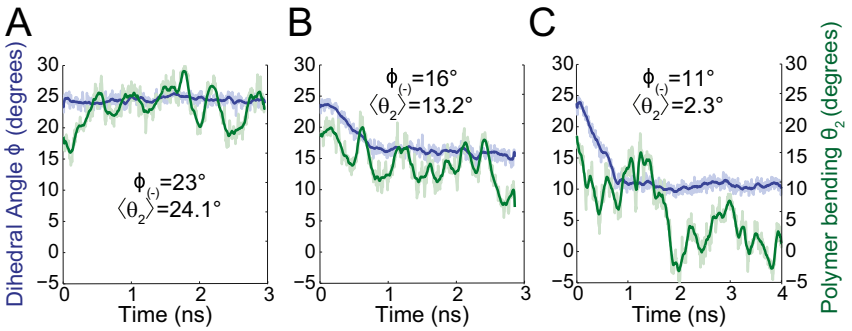

Fig. S6. Steered (–) subunit dihedral values are coupled to dimer bending. In simulations initiated from the equilibrium structure of the unconstrained ATP-bound MreB dimer (simulations 8–10, Table S1), steering the value of the (–) subunit dihedral angle over 1 ns from 23° to 23°, 16°, or 11° (*A*, *B*, and *C*, respectively) resulted in an inverse change in bending between the (–) and (+) subunit in the θ_2 direction. Dark curves represent time-smoothed trajectories of the light curves. The final dihedral value of the steered (–) subunit and the equilibrium average value of the intermonomer bending are given for each simulation.

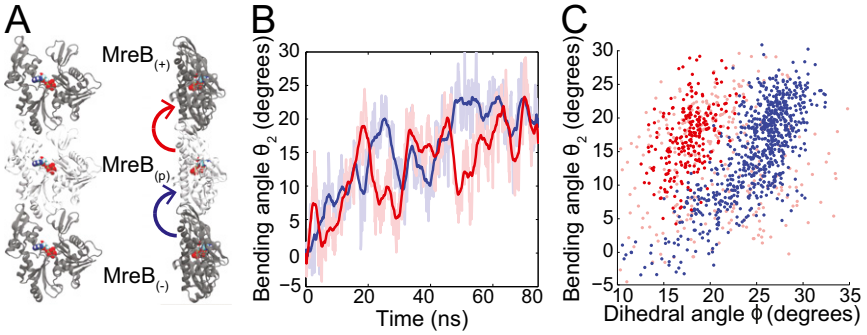

Fig. S7. Trimer simulations of MreB exhibit bending and intersubunit coupling. (*A*) Simulations of an MreB trimer bound to ATP behaved similarly to simulations of MreB dimers. The trimer simulation was stable over the time course of the simulation (74.5 ns). The middle subunit [$MreB_{(p)}$] did not behave differently than top and bottom subunits [$MreB_{(+)}$ and $MreB_{(-)}$ respectively]. (*B*) In agreement with our observations in MreB dimer simulations, the trimer had larger-scale bending along the second bending axis θ_2 between both pairs of subunits [between $MreB_{(-)}$ and $MreB_{(p)}$, and between $MreB_{(p)}$ and $MreB_{(+)}$]. (*C*) Both pairs of subunits exhibited coupling between the flatness of the lower subunit of the pair and dimer bending, also in agreement with dimer simulations. The upper pair transiently loses this coupling (light red, 10–40 ns) when the (+) subunit transiently adopts an open state (Fig. S2). Upon closing, this coupling is reestablished (dark red, 50–75 ns). The lower pair exhibits flatness-bending coupling throughout the entire simulation.

Table S1. Description of MD simulations

No.	Name	Structure	Ligand	Atoms (× 1,000)	Condition	Time, ns
1	G-MreB ATP Mg^{2+}	PDB: 1JCG monomer	ATP and Mg^{2+}	62.3	Unconstrained	55.0
2	F-MreB ATP Mg^{2+}	PDB: 1JCG dimer	2× ATP and 2× Mg^{2+}	95.1	Unconstrained	140.6
3	G(+)-F(–)-MreB ATP Mg^{2+}	(+): Equilibrium structure from 1 (–): PDB: 1JCG	2× ATP and 2× Mg^{2+}	117.7	Unconstrained	66.3
4	G-MreB ATP	PDB: 1JCG monomer	ATP	71.8	Unconstrained	40.0
5	F-MreB ATP	PDB: 1JCG dimer	2× ATP	95.1	Unconstrained	140.6
6	G-MreB ADP Mg^{2+}	PDB: 1JCG monomer	ADP and Mg^{2+}	62.3	Unconstrained	62.9
7	F-MreB ADP Mg^{2+}	PDB: 1JCG dimer	2× ADP and 2× Mg^{2+}	95.1	Unconstrained	65.0
8	F-MreB ATP Mg^{2+} ϕ steer 11	Equilibrium structure from 3, with $\phi_{(-)}$ steered from 23 to 11	2× ATP and 2× Mg^{2+}	138.3	Steered	4.0
9	F-MreB ATP Mg^{2+} ϕ steer 16	Equilibrium structure from 3, with $\phi_{(-)}$ steered from 23 to 16	2× ATP and 2× Mg^{2+}	138.3	Steered	3.0
10	F-MreB ATP Mg^{2+} ϕ steer 26	Equilibrium structure from 3, with $\phi_{(-)}$ steered from 23 to 23	2× ATP and 2× Mg^{2+}	138.3	Steered	3.0
11	G(+)-F(–)-MreB ATP Mg^{2+} $\phi = 11$	Same as 8, with $\phi_{(-)}$=11	2× ATP and 2× Mg^{2+}	117.7	Constrained	33.4
12	G(+)-F(–)-MreB ATP Mg^{2+} $\phi = 15$	Same as 8, with $\phi_{(-)}$=15	2× ATP and 2× Mg^{2+}	105.5	Constrained	35.0
13	G(+)-F(–)-MreB ATP Mg^{2+} $\phi = 21$	Same as 8, with $\phi_{(-)}$=21	2× ATP and 2× Mg^{2+}	105.5	Constrained	35.3
14	F-MreB ATP Mg^{2+} trimer	PDB: 1JCF trimer	3× ATP and 3× Mg^{2+}	143.9	Unconstrained	74.5

All simulations were performed in explicit water with neutralizing salt conditions. Further simulation conditions are given in *Methods*. Simulations of MreB as a monomer and dimer are referred to as G-MreB and F-MreB, respectively. In dimer simulations, the bottom and top subunits are referred to as the (–) and (+) subunits, respectively. Unconstrained simulations do not have any external forces other than from random thermal noise. In steered simulations, the (–) subunit dihedral angle is steered over the first 1 ns between the two values given in the structure column. In constrained simulations, the (–) subunit is constrained to a specific dihedral angle given in the structure column. All simulations except the trimer simulation were replicated at least twice to ensure repeatability of measurements.

Table S2. Residue definitions of MreB subdomains

Subdomain	*Thermotoga maritima* residues, aa	Color
IB	1–29, 73–138, 315–336	Yellow
IA	30–72	Blue
IIA	139–175, 250–314	Red
IIB	176–249	Green

Residues of MreB subdomains are defined in ref. 1.

Table S3. Mean bending orientations and stiffnesses (bending rigidities) of F-MreB in MD simulations

	Orientations			Bending modulus in k_BT/radians^2		
Simulation	Bend 1 θ_1, °	Bend 2 θ_2, °	Twist θ_3, °	k_1	k_2	k_3
F-MreB ATP Mg^{2+}	4.0	26.0	0.3	196	196	820
F-MreB ADP Mg^{2+}	3.1	8.6	–3.3	328	164	460

Measures of bending orientation were repeatable for ADP-bound simulations. Owing to the large conformational changes, not all repetitions of ATP-bound simulations equilibrated to the same final value of θ_2. However, all repeat simulations of ATP-bound F-MreB exhibited larger bending than simulations of ADP-bound F-MreB, suggesting that extended simulation would lead to similar bending angles.

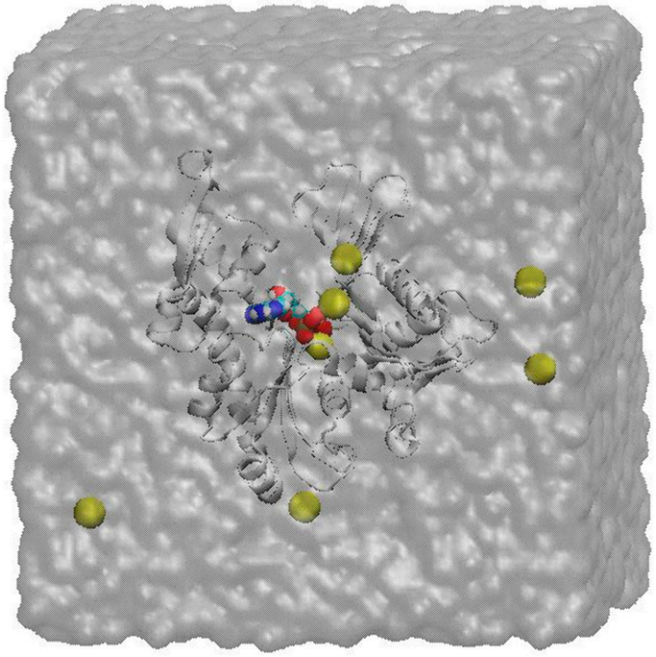

Movie S1. Dynamics of the opening of monomeric MreB bound to ATP and in the presence of Mg^{2+} (simulation 1).

Movie S1

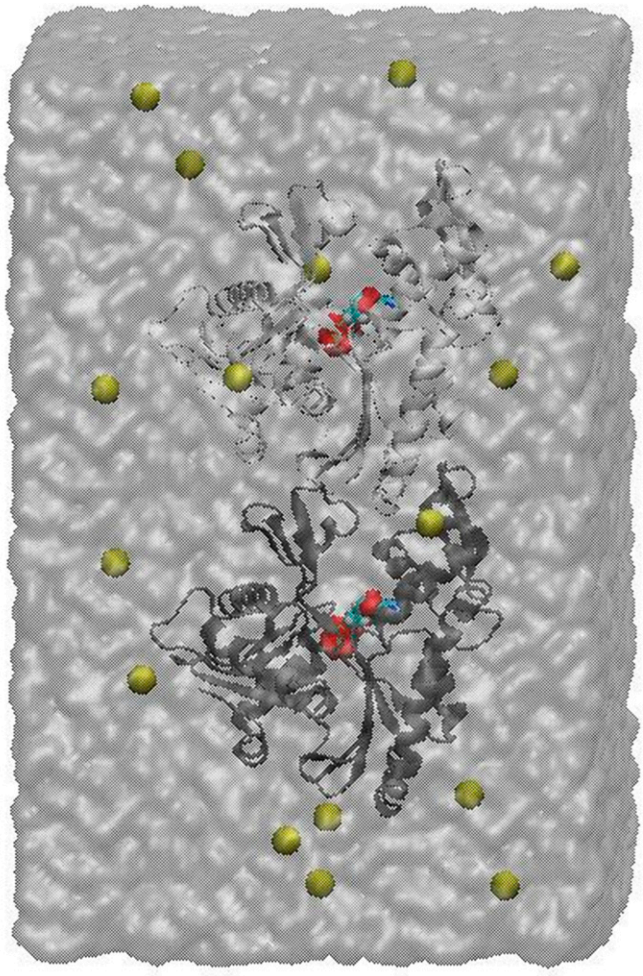

Movie S2. Dynamics of ATP leaving its binding pocket in the absence of Mg^{2+} (simulation 5).

Movie S2

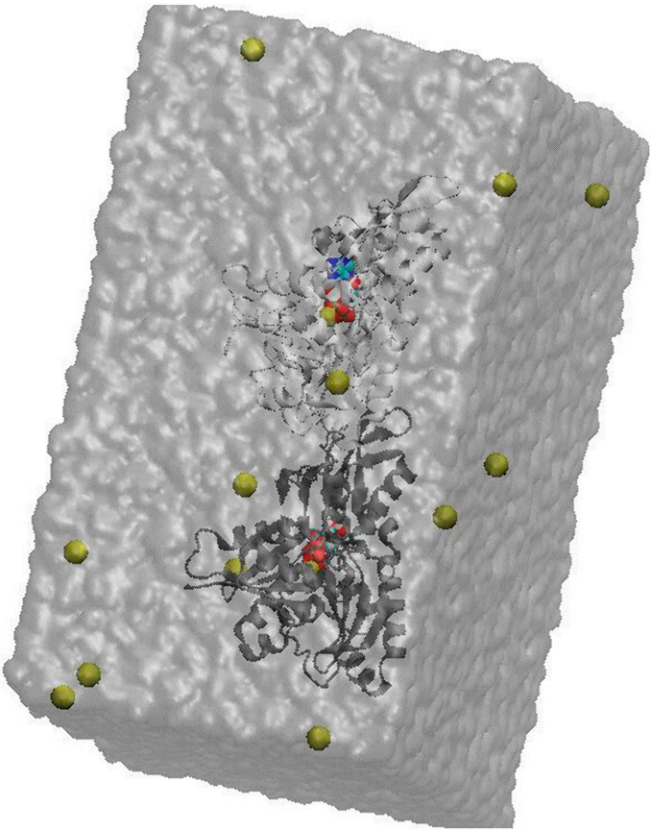

Movie S3. Dynamics of steered (–) subunit dihedral angle coupled to dimer bending (simulation 8).

Movie S3